Above-bandgap voltages from ferroelectric photovoltaic devices

S. Y. Yang[1]*, J. Seidel[2,3], S. J. Byrnes[2,3], P. Shafer[1], C.-H. Yang[3], M. D. Rossell[4], P. Yu[3], Y.-H. Chu[5], J. F. Scott[6], J. W. Ager, III[2], L. W. Martin[2] and R. Ramesh[1,2,3]

In conventional solid-state photovoltaics, electron–hole pairs are created by light absorption in a semiconductor and separated by the electric field spaning a micrometre-thick depletion region. The maximum voltage these devices can produce is equal to the semiconductor electronic bandgap. Here, we report the discovery of a fundamentally different mechanism for photovoltaic charge separation, which operates over a distance of 1–2 nm and produces voltages that are significantly higher than the bandgap. The separation happens at previously unobserved nanoscale steps of the electrostatic potential that naturally occur at ferroelectric domain walls in the complex oxide $BiFeO_3$. Electric-field control over domain structure allows the photovoltaic effect to be reversed in polarity or turned off. This new degree of control, and the high voltages produced, may find application in optoelectronic devices.

The conversion process of light energy to electrical energy in photovoltaic devices relies on some form of built-in asymmetry that leads to the separation of electrons and holes. The fundamental physics behind this effect (for example, in silicon-based cells) is charge separation using the potential developed at a p–n junction, or heterojunction[1-3]. This suggests the following question—are there other pathways to accomplish charge separation in materials to enable the next generation of photovoltaics? In the past, anomalous photovoltaic effects in polar materials have been found to arise from two mechanisms: (i) granularity[4,5] and (ii) the inherent non-centrosymmetry in the bulk material, that is, the absence of an inversion centre of symmetry[6-9]. The former mechanism inevitably suffers from the granular interface being poorly controlled, and the latter is typically seen in wide-bandgap semiconductors ($E_g > 2.5$ eV), which absorb very little of the visible spectrum. In this paper, we describe a new mechanism of charge separation and photovoltage generation that occurs exclusively at nanometre-scale ferroelectric domain walls in a model ferroelectric, $BiFeO_3$ (BFO), under white-light illumination. In contrast to semiconductor-based photovoltaics[10], the photovoltages observed here are significantly higher than the electronic bandgap.

The rhombohedrally distorted perovskite structure of BFO leads to eight ferroelectric polarization directions along the pseudocubic 111-directions, corresponding to four structural variants. The possible domain pattern formation in (001)-oriented epitaxial rhombohedral perovskite ferroelectric films and their control has been well established by earlier theoretical and experimental studies[11-13]. To eliminate confusion, we use the notation set prescribed in ref. 11. Domain walls in such materials are typically 1–2 nm wide[14]. Additionally, recent studies have demonstrated that BFO has a direct bandgap of ~2.67 eV (~465 nm)[15] and has been previously shown to display a conventional photovoltaic effect (open-circuit voltage $V_{OC} \ll E_g$)[16] and photoconductivity[15].

The details of the growth of the BFO thin films used in our study are given in the Methods. Piezoresponse force microscopy (PFM) reveals that ordered arrays of 71° (Fig. 1a and schematically depicted in Fig. 1b) and 109° domain walls with two in-plane variants (Fig. 1c and schematically in Fig. 1d) have been created through such a careful heteroepitaxial growth process. X-ray diffraction studies (insets of Fig. 1a,c) confirm the presence of these two different types of domain wall[17]. Additional X-ray diffraction reciprocal-space-mapping studies (Supplementary Fig. S1) reveal the high quality of these ordered stripe domains. In both cases, there is a net polarization aligned in the plane of the film, that is, perpendicular to the projection of the domain wall plane on the (001) film surface (Fig. 1b,d). Transmission electron microscopy (TEM) images of the two different domain structures show that the 71° domain walls (Supplementary Fig. S2a) lie along 101-type planes, whereas the 109° domain walls (Supplementary Fig. S2b) lie along 100-type planes, consistent with theoretical predictions[11]. Detailed analyses of the atomic structure at these domain walls reveal a wall width of 1–2 nm, consistent with previous work[14,18]. Such nanoscale domain-wall features are the focus of this work.

Photovoltaic device measurements

Test structures, based on symmetric platinum top electrodes with a length of 500 μm and an inter-electrode distance of 200 μm, were fabricated on top of 100-nm-thick films by photolithography in two geometries: electrodes for electric transport measurements (i) perpendicular ($DW_\perp$) and (ii) parallel ($DW_\parallel$) to the domain walls (DW, Fig. 2a,b, respectively). Current–voltage (I–V) characteristics of samples in the two geometries, with ordered arrays of 71° domain walls, were measured under saturation illumination (Supplementary Fig. S3) on the same film in both dark- and white-light illumination (285 mW cm⁻² as written but) and reveal strikingly different photovoltaic behaviours (Fig. 2c,d). In the $DW_\perp$ direction, a large photo induced V_{OC} of 16 V was measured, with in-plane short-circuit current density $J_{sc} \approx 1.2 \times 10^{-4}$ A cm⁻². In contrast, dark and light I–V curves measured in the $DW_\parallel$ direction exhibit a significant photoconductivity, but no photo induced V_{OC}.

[1]Department of Materials Science and Engineering, University of California, Berkeley, Berkeley, California 94720, USA, [2]Materials Sciences Division, Lawrence Berkeley National Laboratory, Berkeley, California 94720, USA, [3]Department of Physics, University of California, Berkeley, California 94720, USA, [4]National Center for Electron Microscopy, Lawrence Berkeley National Laboratory, Berkeley, California 94720, USA, [5]Department of Materials Science and Engineering, National Chiao Tung University, HsinChu, Taiwan 30010, [6]Department of Earth Sciences, University of Cambridge, Cambridge CB2 3EQ, UK. *e-mail: syyang@berkeley.edu

143

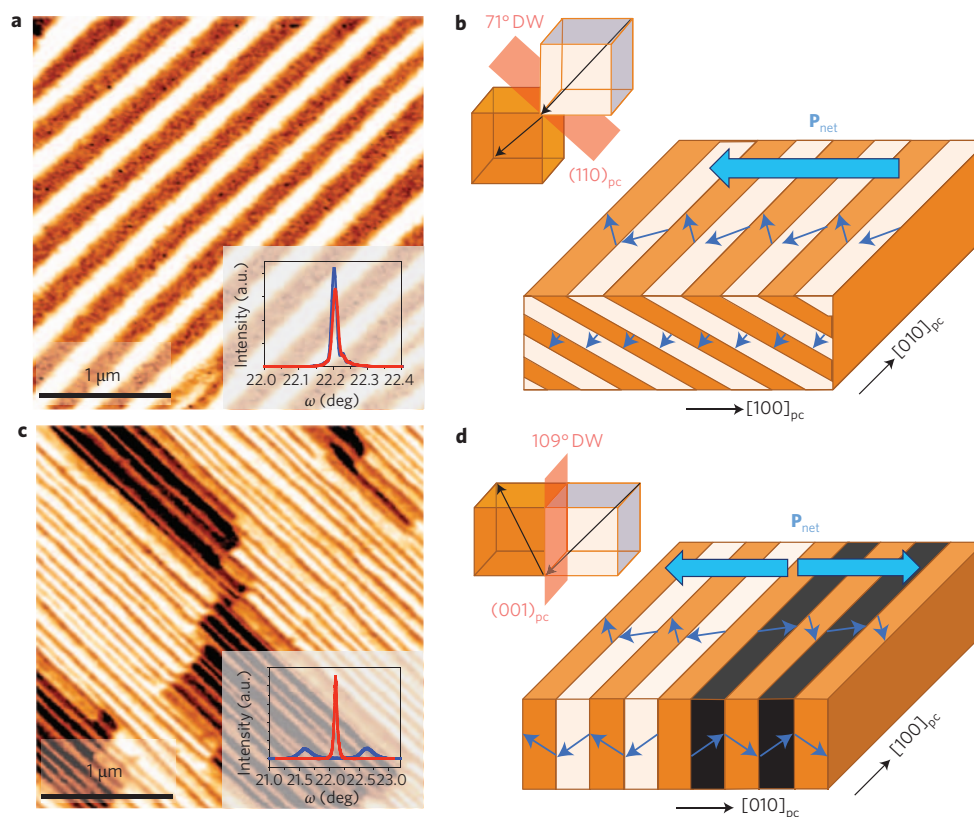**Figure 1 | Model domain-wall architectures. a**, Piezoresponse force microscopy image of ordered arrays of 71° domain walls. Inset: corresponding X-ray rocking curves, along two orthogonal crystal axes, demonstrating the high quality of the films. **b**, Schematic of the 71° domain-wall arrays. The various arrows map out the different components of polarization (both in-plane and out-of-plane) as well as the net polarization direction (large arrow) in the samples. Samples are found to have net polarization in the plane of the film. **c**, Piezoresponse force microscopy image of ordered arrays of 109° domain walls. Inset shows the corresponding X-ray rocking curves, along two orthogonal crystal axes. **d**, Schematic of the 109° domain-wall arrays.
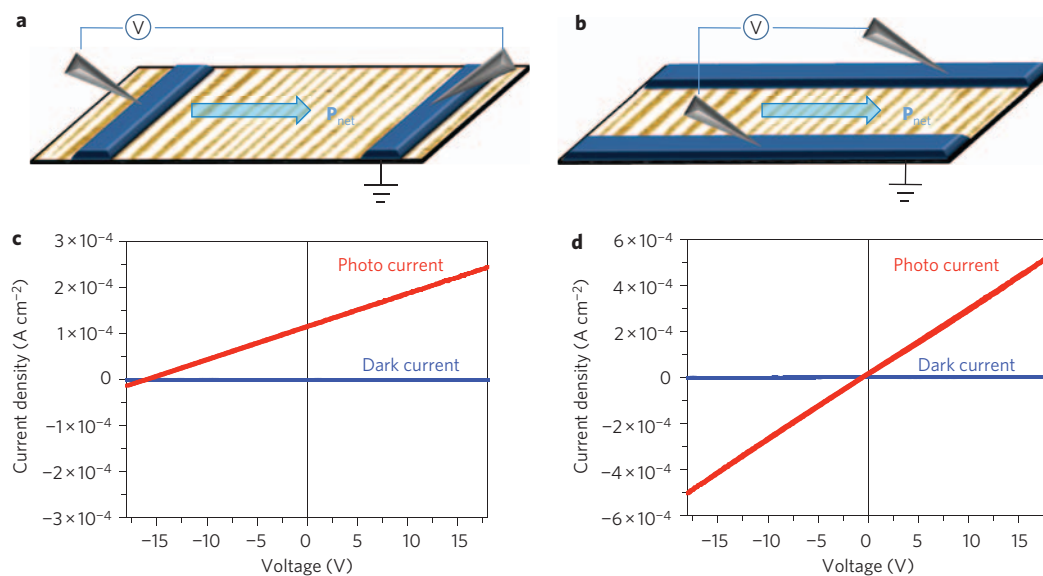

Figure 2 | Light and dark I–V measurements. a,b, Schematics of the perpendicular (DW$_\perp$) (**a**) and the parallel (DW$_\parallel$) (**b**) device geometries. **c,d**, Corresponding I–V measurements of the DW$_\perp$ (**c**) and DW$_\parallel$ (**d**) devices, respectively.

The photo induced voltages were found to increase linearly in magnitude as the electrode spacing was increased (Fig. 3a). Most importantly, a single domain sample (that is, with no domain walls between the platinum contacts; black curve, Fig. 3a) show negligible levels of photovoltage, which rules out a 'bulk' photovoltaic effect arising from non-centrosymmetry[6,7]. In turn, this strongly suggests the prominent role of domain walls in creating the anomalous photovoltages. In fact, the magnitude of the overall potential drop varies linearly with the total number of domain walls between the electrodes (Fig. 3a). The thickness dependence of the
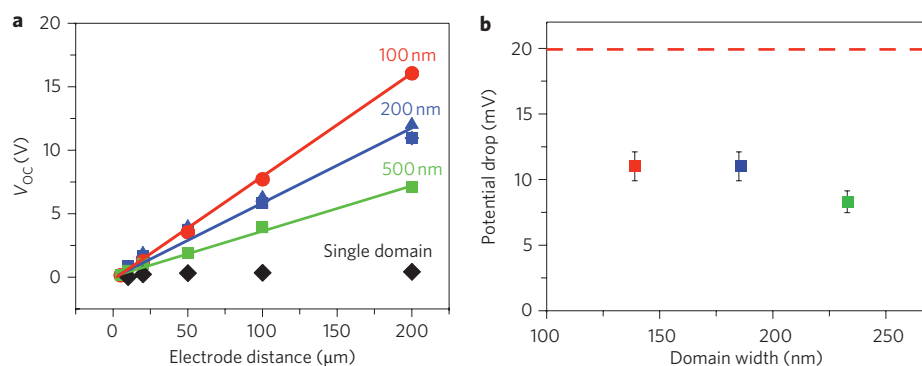
Figure 3 | Role of domain-walls in the photovoltaic response. a, Study of the evolution of V_{OC} as a function of electrode spacing for four different samples: 71° domain-walls samples with thicknesses of 100 nm (red), 200 nm (blue) and 500 nm (green) as well as a monodomain BFO film having no domain walls (black). A clear correlation between the number of domain walls and the magnitude of V_{OC} is observed. **b**, The potential drop in relation to domain-wall width is essentially constant regardless of the spacing between domain walls. The dashed line represents the theoretically expected potential drop per domain wall from ref. 21.

photovoltage provides another route to verify this conclusion, because the wall density scales inversely with film thickness[19,20]. From PFM analysis we have calculated the average domain spacing and used this to calculate the potential drop for each domain wall to be ~10 mV, irrespective of the domain width (Fig. 3b). This value is quite close to the theoretically predicted 20 mV potential drop across 71° domain walls in BFO (ref. 21).

Model for the photovoltaic effect

Figure 4a–d shows our proposed model for the effect described above. Figure 4a is a schematic of the model domain structure showing a series of 71° domain walls. Figure 4b shows the corresponding position of the valence (VB) and conduction (CB) bands in dark conditions. Recent *ab initio* calculations suggest that ferroelectric domain walls have built-in potential steps[14,21] arising from the component of the polarization perpendicular to the domain wall. The associated charge density, $\rho = -\nabla \cdot P$, forms an electric dipole, leading to an electric field within the wall and a potential step from one side to the other. In a strongly correlated, polar system such as BFO, the photo generated exciton is expected to be localized and tightly bound. Therefore, such an exciton in the bulk of the BFO (Fig. 4b(i)), is expected to quickly recombine, resulting in no net photo effect. If the light is incident at the domain wall (Fig. 4b(ii)), the significantly higher local electric field enables a more efficient separation of the excitons, creating a net imbalance in charge carriers near the domain walls and resulting in the band diagram shown in Fig. 4c. This effect (analogous to the type-II band alignment that drives polymeric solar cells) means that, under illumination, a net voltage is observed across the entire sample, resulting from the combined effect of the domain walls and the excess charge carriers created by illumination (Fig. 4d). Photo excited electron–hole pairs are separated and drift to either side of the domain wall, building up an excess of charge. A close inspection of the effects at a given domain wall (Fig. 4) reveals a similar picture to a classic p–n junction. The key difference is the magnitude of the electric field that drives charge separation. In a classic silicon-based system ($V_{OC} \approx 0.7$ V; depletion layer thickness, ~1 μm), an effective electric field of ~7 kV cm^{-1} is obtained (compared with the BFO system, with a field of ~50 kV cm^{-1}) for each domain wall. In open-circuit illuminated conditions, the electric field across the domain walls should decrease relative to its thermal-equilibrium value, creating a drift-diffusion current equal and opposite to the photocurrent described above. The domains themselves maintain the same electric field as in thermal equilibrium, because this is already the correct field for zero net

current. Therefore, a net electric field would build up across the sample (Fig. 4c).

To validate this model, we first rule out the bulk photovoltaic effect previously observed in other ferroelectric crystals such as LiNbO$_3$ (LNO). It is useful to make comparisons with known results on periodically poled LNO, because BFO and LNO have the same symmetry and LNO is an extensively studied photovoltaic ferroelectric material[22]. There have been no reports of large photovoltages being generated in undoped LNO and, because LNO and BFO both have a bulk symmetry $R3c$, this implies that such high-voltage output in the latter is very unlikely to be a bulk property. Additionally, despite possessing the same bulk symmetry, the domain structures in LNO and BFO are very different. LNO has a rhombohedral–rhombohedral crystal class-preserving ferroelectric phase transition. As a result, it cannot be ferroelastic, and only 180° domain walls can exist[23]. These apparently play no part in any large photovoltage output. In contrast, BFO has a rhombohedral–orthorhombic transition at its Curie temperature. This is a ferroelastic phase transition with 71°, 109° and 180° domain walls. Thus, quantitative differences in photovoltaic response suggest the role of either 71° or 109° domain walls.

Finally, we note that the bulk photovoltaic tensor is generally third-rank and non-diagonal in $R3c$ materials such as LNO (ref. 24). Thus, application of an optical field is, in general, affected not only by the r_{33} photovoltaic coefficient[22], but also by the r_{15} coefficient[25]. In a typical experiment on LNO (refs 26,27), this off-diagonal term produces a field of 40 kV cm^{-1} perpendicular to the threefold polar axis for 500 mW of 514.5 nm laser light weakly focused to a 50-μm spot diameter. This number may be compared with those in the present study and suggests that a fully quantitative analysis must involve the full off-diagonal photovoltaic tensor. This was suggested earlier for puzzling results regarding the photovoltaic response in YBaCuO high-T_C materials[28]. We also note that the photovoltaic response perpendicular to the polar threefold axis can be compensated or enhanced by a strong thermal gradient[29–31]. Because certain domain walls conduct electricity in BFO, this could involve local heating[21]. Thus, comparison of the present data with those for LNO supports the argument that the new effects reported here cannot be bulk in nature.

Final evidence of a completely new photovoltaic mechanism comes from the fact that the direction of the measured J_{SC} in our BFO films is parallel to the net in-plane polarization. This current direction is opposite to what has been observed for granular ferroelectric materials[5]. In turn, we have observed that there is a drop in the potential in the direction of the net in-plane polarization in these epitaxial BFO films. The expected magnitude of J_{SC} can be
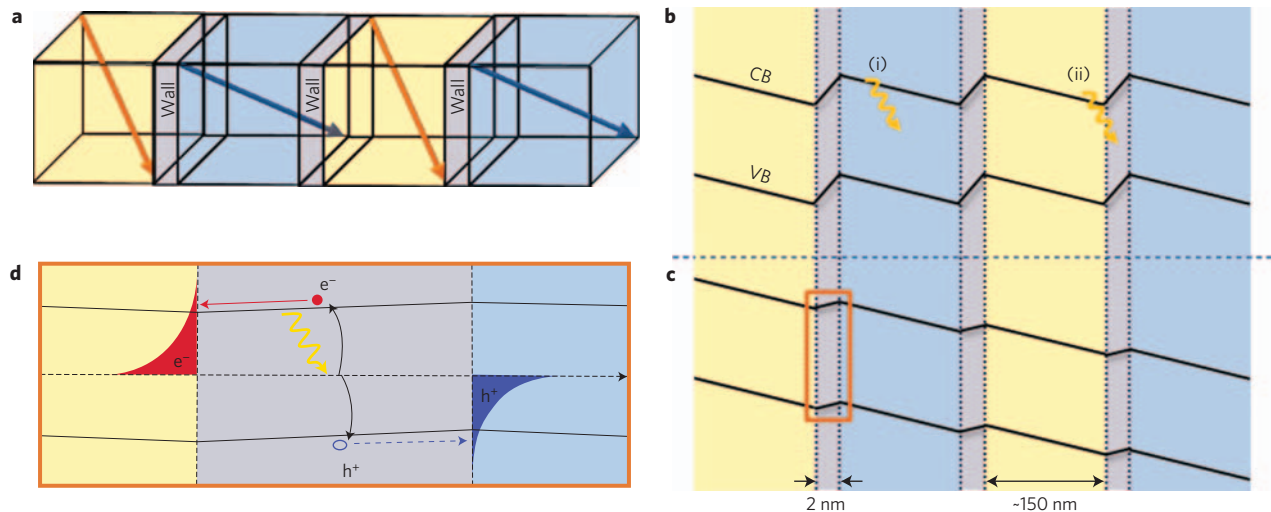
Figure 4 | Band structure in dark conditions and under illumination. a, Schematic of four domains (three domain walls) in an order array of 71° domain walls. **b**, Corresponding band diagram showing the valence band (VB) and conduction band (CB) across these domains and domain walls in the dark. Note that there is no net voltage across the sample in the dark. Section (i) illustrates a photon hitting in the bulk of a domain and section (ii) a photon hitting at a domain wall. **c**, Evolution of band structure upon illumination of the domain wall array. **d**, Detailed picture of the build-up of photo excited charges at a domain wall.
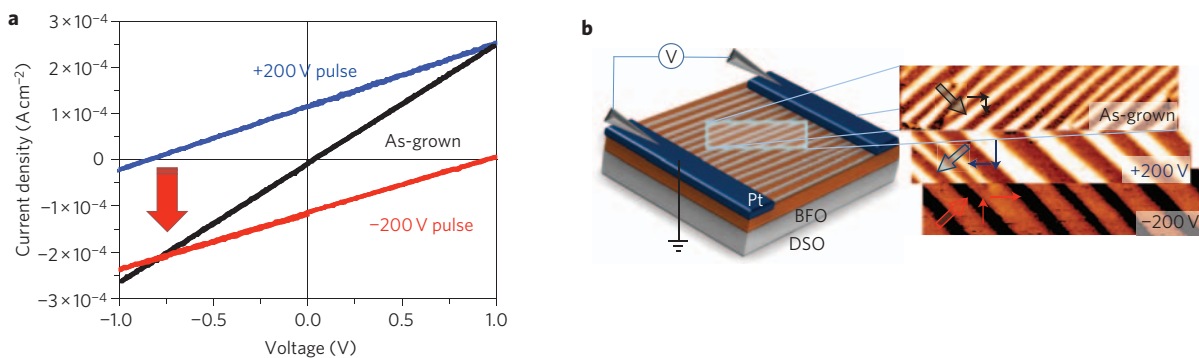

Figure 5 | Domain-wall switching effect. a, Light $I–V$ measurement in the DW$_{\parallel}$ geometry shows no observable photovoltaic effect, as grown. On rotation of the domain structure to the DW$_{\perp}$ configuration after application of ±200 V voltage pulses to the in-plane device structure, a photovoltaic effect is observed. **b**, Corresponding PFM images of the as-grown (top panel), 200 V poled (middle panel), and -200 V poled (bottom panel) device structures. The arrows indicate the in-plane projection of the polarization and the net polarization direction for the entire device structure.

predicted, and is consistent with measurements (details of the calculation are given in the Supplementary Information).

Control of the photovoltaic response by electric fields

To demonstrate an additional level of control of the photovoltaic effect in these films, we have studied the evolution of photovoltaic properties as a function of domain switching in planar device structures. $I–V$ characterization of an as-grown device structure in the DW$_{\parallel}$ geometry is shown in Fig. 5a. Consistent with data in Fig. 2, there is no observable photovoltaic response in this geometry. Using a device spacing of 10 μm, we can then apply voltage pulses of 200 V between the two in-plane electrodes to induce ferroelectric domain switching. Following application of such a field ($E \approx 200$ kV cm^{-1}) for a pulse of 100 μs, a corresponding rotation of the ferroelectric domain structure was observed, thereby creating a system with the DW$_{\perp}$ geometry. Subsequent light $I–V$ measurements reveal the formation of an anomalous photovoltaic effect in this film (blue curve, Fig. 5a). The corresponding PFM image following the $+200$ V pulse reveals that the domain structure is effectively rotated by 90° from the original configuration (Fig. 5b, top and middle panels). It is clear that this domain

configuration is essential to create the potential drop necessary for the anomalous photovoltaic effect. Furthermore, upon application of a -200 V/100 μs pulse, the polarity of the photo-induced voltage and current can be flipped (red curve, Fig. 5a). This is explained by a change in the direction of the net, in-plane polarization of the BFO film (Fig. 5b, bottom panel).

Our earlier theoretical work showed that the magnitude of the potential step is higher in the case of 109° domain walls (150 mV, compared to 20 mV for 71° domain walls). We were constrained in terms of a macroscopic measurement of the 109° domain samples due to the presence of a random distribution of the two in-plane variants. We therefore carried out microscopic measurements (details of measurements are given in Supplementary Fig. S4), which revealed an ~4× larger potential drop per domain wall compared to the 71° walls.

Conclusion

In summary, we have shown that a photovoltaic effect in BFO thin films arises from a unique, new mechanism—namely, structurally driven steps of the electrostatic potential at nanometre-scale domain walls. These potential steps, which had been hypothesized,

had never before been observed directly. By controlling the domain structure in such BFO films we can, in turn, gain control over the photo properties of these materials.

Methods

Thin-film growth. BFO films with thicknesses between 100 and 500 nm were grown on single-crystalline (110) $DyScO_3$ (DSO) substrates by metal–organic chemical vapour deposition (MOCVD)[32]. Annealing treatments of the DSO substrates (1,200 °C for 3 h in flowing O_2) produced ordered arrays of unit-cell-high terraces on the substrate surface. Growth on such annealed substrates results in ordered arrays of 71° domain walls, and growth on un-annealed substrates gives rise to ordered arrays of 109° domain walls.

References

1. Ginley, D., Green, M. A. & Collins, R. Solar energy conversion toward 1 terawatt. *Mater. Res. Soc. Bull.* **33,** 355–364 (2008).
2. Gur, I., Fromer, N. A., Geier, M. L. & Alivisatos, A. P. Air-stable all-inorganic nanocrystal solar cells processed from solution. *Science* **310,** 462–465 (2005).
3. O'Regan, B. & Grätzel, M. A low-cost, high-efficiency solar cell based on dye-sensitized colloidal TiO_2 films. *Nature* **353,** 737–740 (1991).
4. Goldstein, B. & Pensak, L. High-voltage photovoltaic effect. *J. Appl. Phys.* **30,** 155–161 (1959).
5. Brody, P. S. & Crowne, F. Mechanism for the high voltage photovoltaic effect in ceramic ferroelectrics. *J. Electron. Mater.* **4,** 955–971 (1975).
6. Glass, A. M., von der Linde, D. & Negran, T. J. High-voltage bulk photovoltaic effect and the photorefractive process in $LiNbO_3$. *Appl. Phys. Lett.* **25,** 233–235 (1974).
7. Fridkin, V. M. Bulk photovoltaic effect in noncentrosymmetric crystals. *Crystallogr. Rep.* **46,** 654–658 (2001).
8. Ichiki, M., Furue, H., Kobayashi, T. & Maeda R. Photovoltaic properties of $(Pb,La)(Zr,Ti)O_3$ films with different crystallographic orientations. *Appl. Phys. Lett.* **87,** 222903 (2005).
9. Ichiki, M. *et al.* Photovoltaic effect of lead lanthanum zirconate titanate in a layered film structure design. *Appl. Phys. Lett.* **84,** 395–397 (2004).
10. Shockley, W. & Queisser, H. J. Detailed balance limit of efficiency of p–n junction solar cells. *J. Appl. Phys.* **32,** 510–519 (1975).
11. Streiffer, S. K. *et al.* Domain patterns in epitaxial rhombohedral ferroelectric films. I. Geometry and experiments. *J. Appl. Phys.* **83,** 2742–2753 (1998).
12. Iwata, M. *et al.* Domain wall structure in $Pb(Zn_{1/2}Nb_{2/3})O_3$-$PbTiO_3$-mixed crystals by atomic force microscopy. *Jpn J. Appl. Phys.* **43,** 6812–6815 (2004).
13. Chu, Y.-H. *et al.* Domain control in multiferroic $BiFeO_3$ through substrate vicinality. *Adv. Mater.* **19,** 2662–2666 (2007).
14. Meyer, B. & Vanderbilt, D. *Ab initio* study of ferroelectric domain walls in $PbTiO_3$. *Phys. Rev. B* **65,** 104111 (2002).
15. Basu, S. R. *et al.* Photoconductivity in $BiFeO_3$ thin films. *Appl. Phys. Lett.* **92,** 091905 (2008).
16. Choi, T., Lee, S., Choi, Y. J., Kiryukhin, V. & Cheong, S.-W. Switchable ferroelectric diode and photovoltaic effect in $BiFeO_3$. *Science* **324,** 63–66 (2009).
17. Chu, Y.-H. *et al.* Nanoscale control of domain architectures in $BiFeO_3$ thin films. *Nano Lett.* **9,** 1726–1730 (2009).
18. Lubk, A., Gemming, S. & Spaldin, N. A. First-principles study of ferroelectric domain walls in multiferroic bismuth ferrite. *Phys. Rev. B* **80,** 104110 (2009).
19. Romanov, A. E., Lefevre, M. J., Speck, J. S., Pompe, W. & Streiffer, S. K. Domain pattern formation in epitaxial rhombohedral ferroelectric films. II. Interfacial defects and energetic. *J. Appl. Phys.* **83,** 2754–2765 (1998).
20. Chen, Y. B. *et al.* Ferroelectric domain structures of epitaxial (001) $BiFeO_3$ thin films. *Appl. Phys. Lett.* **90,** 072907 (2007).
21. Seidel, J. *et al.* Conduction at domain walls in oxide multiferroics. *Nature Mater.* **8,** 229–234 (2009).
22. Lines, M. E. & Glass, A. M. *Principles and Applications of Ferroelectrics and Related Materials* (Clarendon Press, 1977).
23. Toledano, J.-C. Ferro-elasticity. *Ann. Telecommun.* **29,** 249–270 (1974).
24. Chen, F. S., LaMacchia, J. T. & Fraser, D. B. Holographic storage in lithium niobate. *Appl. Phys. Lett.* **13,** 223–225 (1968).
25. Odulov, S. G. Spatially oscillating photovoltaic current in iron-doped lithium niobate crystals. *JETP Lett.* **35,** 10–12 (1982).
26. Anikiev, A. A., Reznik, L. G., Umarov, B. S. & Scott, J. F. Perturbed polariton spectra in optically damaged $LiNbO_3$. *Ferroelec. Lett.* **3,** 89–96 (1985).
27. Chaib, H., Otto, T. & Eng, L. M. Electrical and optical properties of $LiNbO_3$ single crystals at room temperature. *Phys. Rev. B* **67,** 174109 (2003).
28. Scott, J. F. Interpretation of photovoltaic pulses in normal $YBa_2Cu_3O_7$. *Appl. Phys. Lett.* **56,** 1914–1915 (1990).
29. Reznik, L. G., Anikiev, A. A., Umarov, B. S. & Scott, J. F. Studies of optical damage in lithium niobate in the presence of thermal gradients. *Ferroelectrics* **64,** 215–219 (1985).
30. Kostritskii, S. M., Sevostyanov, O. G., Aillerie, M. & Bourson, P. Suppression of photorefractive damage with aid of steady-state temperature gradient in nominally pure $LiNbO_3$ crystals. *J. Appl. Phys.* **104,** 114104 (2008).
31. Kostritskii, S. M., Bourson, P., Mouras, R. & Fontana, M. D. Optical fatigue of undoped lithium niobate crystals caused by irreversible photorefractive damage at high-intensity illumination. *Opt. Mater.* **29,** 732–737 (2007).
32. Yang, S. Y. *et al.* Metalorganic chemical vapor deposition of lead-free ferroelectric $BiFeO_3$ films for memory applications. *Appl. Phys. Lett.* **87,** 102903 (2005).

Author contributions

S.Y.Y. and J.S. conceived and designed the experiments. S.Y.Y., J.S. and S.J.B. performed the experiments. P.S., C.H.Y., M.D.R., P.Y., Y.-H.C. and J.W.A. contributed material and analysis. S.Y.Y., J.S., S.J.B., J.F.S., L.W.M. and R.R. co-wrote the paper.

Additional information

The authors declare no competing financial interests. Supplementary information accompanies this paper at www.nature.com/naturenanotechnology. Reprints and permission information is available online at http://npg.nature.com/reprintsandpermissions/. Correspondence and requests for materials should be addressed to S.Y.Y.